# Power Boosting of Strongly Coupled Wireless Power Transfer Systems by Aligning 1st/3rd Harmonic Frequencies With Splitting Frequencies

Bowang Zhang, Youhao Hu, Weikang Hu, and Wei Han, *Member, IEEE*

***Abstract*—This letter proposes a novel power-boosting strategy for strongly coupled wireless power transfer system by aligning the first and third harmonic frequencies of the inverter switching node voltage with the lower and upper splitting frequencies, respectively. Within the parity-time symmetric region, the output power at splitting frequencies significantly exceeds that at the natural resonant frequency. Additionally, when the coupling coefficient k is larger than 0.8, the output power can be further enhanced by superimposing the first and third harmonic voltages of the inverter, all while maintaining high efficiency. Finally, experimental results demonstrate that the proposed strategy achieves an output power of 609.2 W, 124.32 times greater than that of 4.9 W at the natural resonant frequency. And the efficiency by using the proposed strategy is 87.04%, which is comparable to the efficiency of 89.91% by operating at the natural resonant frequency.**

***Index Terms*—Parity-time (PT) symmetric, power-boosting, splitting frequency, strongly coupled, voltage superposition.**

## I. Introduction

IN ROTARY applications, a noncontact sliding system utilizing strongly coupled wireless power transfer (WPT) technology eliminates mechanical wear and provides electrical isolation for efficient power transmission [1]. However, the proximity of the transmitter and receiver in the rotating slider results in low power output at the natural resonant frequency, limiting high-power transmission capabilities [2]. Precise model based on differential equations for strongly coupled WPT systems with *LCC–LCC* compensation compared with first harmonic approximation (FHA) is proposed in [3]. However, the current distortion and third harmonic near a coupling coefficient of 0.889 lead to reduced efficiency and higher coil current ratings. SN [4] and *LCL*-N [5] topologies are proposed for creating a more compact and lightweight receiver by eliminating the receiver-side compensation. Nevertheless, issues such as low output power and significant current distortion persist.

Received 12 December 2024; revised 21 January 2025; accepted 7 February 2025. Date of publication 21 February 2025; date of current version 14 April 2025. This work was supported by Guangzhou-HKUST(GZ) Joint Funding Program under Grant 2024A03J0618 and Grant 2024A03J0680. *(Corresponding author: Wei Han.)*

The authors are with the Sustainable Energy and Environment Thrust, The Hong Kong University of Science and Technology, Guangzhou 511453, China (e-mail: bzhang794@connect.hkustgz.edu.cn; yhu543@connect.hkust-gz.edu.cn; wk.hu@connect.ust.hk; weihan@hkust-gz.edu.cn).

Color versions of one or more figures in this article are available at https://doi.org/10.1109/TPEL.2025.3544291.

Digital Object Identifier 10.1109/TPEL.2025.3544291

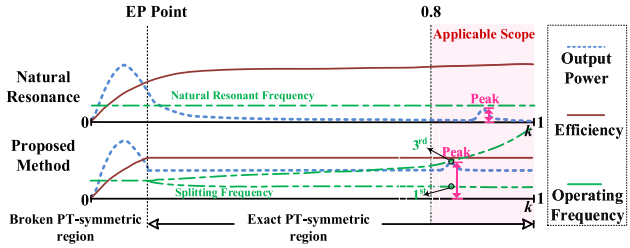


Fig. 1. Applicable scope of proposed power boosting method.

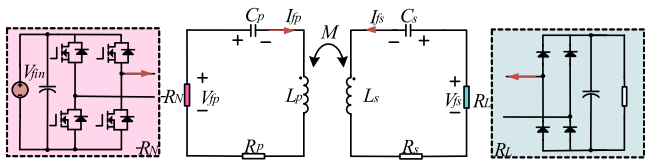


Fig. 2. Equivalent circuit of the PT-symmetric WPT system.

The WPT system will enter the parity-time (PT)-symmetric region when the mutual inductance is larger than the critical coupling condition [6], [7]. Although the output power capability under PT condition has improved compared to its performance at natural resonant frequency, it remains limited [8]. Strong coupling system accompanies high harmonic currents, and thus the output power will deviate from the theoretical value estimated by FHA, making it difficult for implementing the precise output power control. Thus, the low output power of PT-symmetric WPT systems remains a pressing issue that significantly restricts practical applications.

This letter attempts to solve this issue by presenting a power boosting strategy for the PT-symmetric WPT system, the key is to align first/third harmonics frequencies of square voltage with the lower and upper splitting frequencies, respectively. This alignment creates two virtual channels for the simultaneous transfer of energy from both first and third harmonics. In Fig. 1, the applicable scope is when $k$ exceeds 0.8. Compared to the superimposed output mode of first/third harmonics utilizing natural resonance, the proposed method significantly enhances the peak power while maintaining transmission efficiency.

## II. Principle of the Power Boosting Strategy

### A. First Harmonic Approximation (FHA)-Based Model

The input source in the SS compensated PT-symmetric WPT system can be equivalent to a negative resistance $-R_N$, as depicted in Fig. 2. By using the FHA model and considering the first

harmonic voltages ($\boldsymbol{V_{fp}}$ and $\boldsymbol{V_{fs}}$) and currents ($\boldsymbol{I_{fp}}$ and $\boldsymbol{I_{fs}}$) on both sides, the system equation can be derived in (1), where $\omega$, $k$, $L_p$, $L_s$, $R_p$, $R_s$, $C_p$, $C_s$ are the operating frequency, coupling coefficient, coil inductances and internal resistances as well as the compensated capacitors on the primary and secondary sides. Then the resonant frequency $\omega_0$ is $\omega_0 = \frac{1}{\sqrt{L_pC_p}} = \frac{1}{\sqrt{L_sC_s}}$

$$\begin{pmatrix} \frac{-R_N+R_p}{L_p} + j(\omega - \frac{\omega_0^2}{\omega}) & j\omega k\sqrt{\frac{L_p}{L_s}} \\ j\omega k\sqrt{\frac{L_s}{L_p}} & \frac{R_L+R_p}{L_s} + j(\omega - \frac{\omega_0^2}{\omega}) \end{pmatrix} \times \begin{pmatrix} \boldsymbol{I_{fp}} \\ \boldsymbol{I_{fs}} \end{pmatrix} = 0. \quad (1)$$

To calculate the non-zero solution of frequency $\omega$, the real and imaginary parts of coefficient matrix determinant in (1) can be obtained as

$$\begin{cases} \frac{(-R_N+R_p)(R_s+R_L)}{L_pL_s\omega_0^2} - \left(\omega - \frac{\omega_0^2}{\omega}\right) + \omega^2k^2 = 0 \\ \left(\omega - \frac{\omega_0^2}{\omega}\right)\left(\frac{-R_N+R_p}{L_p\omega_0} + \frac{R_s+R_L}{L_s\omega_0}\right) = 0 \end{cases}. \quad (2)$$

By solving (2), the zero-phase-angle (ZPA) operating frequency $\omega_{\mathrm{ZPA}}$ can be calculated by

$$\omega_{(\mathrm{ZPA})} = \begin{cases} \omega_0 & (k < k_c) \\ \omega_0\sqrt{\frac{2-Q_s^{-2}\pm\sqrt{(2-Q_s^{-2})^2+4(k^2-1)}}{2(1-k^2)}} & (k_c \le k < 1) \end{cases} \quad (3)$$

where $Q_s = \frac{\omega_0 L_s}{R_s+R_L}$ is the quality factor of the secondary coil, $k_c = \sqrt{Q_s^{-2} - \frac{Q_s^{-4}}{4}}$ is the critical coupling coefficient.

The $k_c$ divides the WPT system into two regions: the exact PT-symmetric region ($k_c \le k < 1$) and broken PT-symmetric ($0 < k < k_c$) region, which have different characteristics.

1) Exact PT-Symmetric Region: based on (2), when the ZPA operating frequency $\omega_{\mathrm{ZPA}}$ is not equal to $\omega_0$, the negative resistance $-R_N$ in this region can be calculated as

$$-R_N = -\frac{L_p}{L_s}(R_L + R_s) - R_p. \quad (4)$$

By submitting (4) into (1), the ratio of currents on both sides can be given by

$$\frac{\boldsymbol{I_{PT-fs}}}{\boldsymbol{I_{PT-fp}}} = \left|\frac{\boldsymbol{I_{PT-fs}}}{\boldsymbol{I_{PT-fp}}}\right| = \sqrt{\frac{L_p}{L_s}}. \quad (5)$$

The output power $P_{PT\text{-}f}$ and transfer efficiency $\eta_{PT\text{-}f}$ within this region can be obtained as

$$P_{PT-f} = \boldsymbol{I^2_{PT-fs}}R_L = \frac{\boldsymbol{V^2_{fin}}R_L}{\frac{L_p}{L_s}(R_L+R_s)^2 + 2R_p(R_L+R_s) + \frac{L_s}{L_p}R_p^2} \quad (6)$$

$$\eta_{PT-f} = \frac{R_L}{R_L + R_s + \frac{L_s}{L_p}R_p}. \quad (7)$$

According to (5), (6), and (7), the current ratio, output power and efficiency are independent of the coupling coefficient $k$.

2) *Broken PT-Symmetry Region*: there is only one solution $\omega_0$ (natural resonant frequency) for the ZPA operation. The negative resistance $-R_N$ in this region can be given by

$$-R_N = -\frac{\omega_0^2k^2L_pL_s}{R_L+R_s} - R_p. \quad (8)$$

Then the current ratio can be obtained by submitting (8) into (1)

$$\left|\frac{\boldsymbol{I_{N-fp}}}{\boldsymbol{I_{N-fs}}}\right| = \left|\sqrt{\frac{L_s}{L_p}}\left(\frac{1-\frac{\omega_0^2}{\omega^2}}{k} - j\frac{R_L+R_s}{\omega L_s k}\right)\right|_{(\omega=\omega_0)} = \frac{R_L+R_s}{\omega_0 k\sqrt{L_pL_s}}. \quad (9)$$

Within this region, the output power $P_{N\text{-}f}$ and transfer efficiency $\eta_{N\text{-}f}$ at the resonant frequency $\omega$ can be obtained as

$$P_{N-f} = \boldsymbol{I^2_{N-fs}}R_L = \frac{\boldsymbol{V^2_{fin}}R_L\omega_0^2k^2L_pL_s}{[R_p(R_L+R_s) + \omega_0^2k^2L_pL_s]^2} \quad (10)$$

$$\eta_{N-f} = \frac{R_L\omega_0^2k^2L_pL_s}{R_p(R_L+R_s)^2 + (R_L+R_s)\omega_0^2k^2L_pL_s}. \quad (11)$$

### B. Analysis of the Output Characteristics

As derived from (6) and (10), the output power curves under the variation of both coupling coefficient and load resistance within the exact PT region (in red) and the broken PT region (in black) are plotted in Fig. 3(a) based on the key parameters in Table I. It is evident that an increase in coupling coefficient significantly diminishes the output power capability at the natural resonant frequency. While operating at splitting frequencies

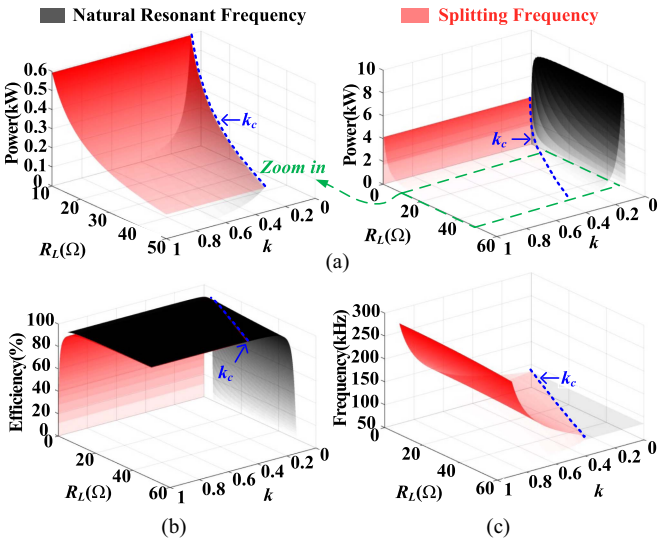


Fig. 3. Output characteristics with different coupling coefficients and load resistances. (a) Output power ($0<R_L<60$). (b) Transfer efficiency ($0<R_L<60$). (c) Operating frequency ($0<R_L<60$).

TABLE I
KEY PARAMETERS OF THE PT-SYMMETRIC WPT SYSTEM

| Item | Value | Item | Value |
|---|---|---|---|
| $L_p/L_s$ | 275 uH | $V_{fin}$ | 80 V |
| $R_p/R_s$ | 0.191 Ω | $k$ | 0–1 |
| $C_p/C_s$ | 12.75 nF | $R_L$ | 0–50 Ω |

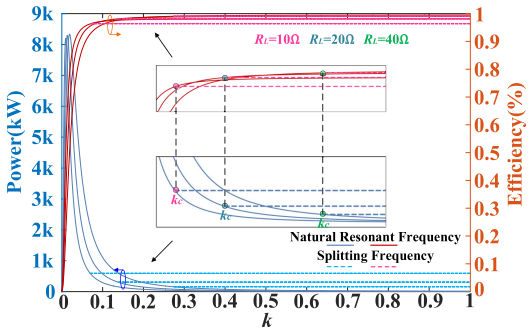


Fig. 4. Output power and transfer efficiency curves with different $R_L$ versus coupling coefficient.

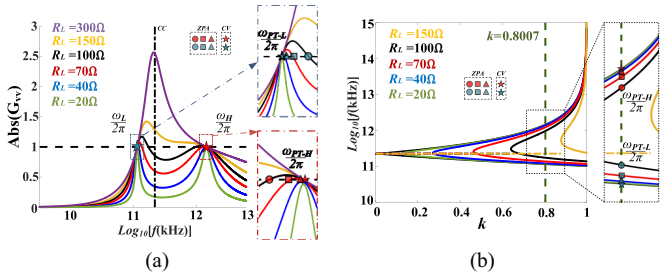


Fig. 5. (a) Voltage transfer ratio versus operating frequency ($k = 0.8007$). (b) Operating frequency versus $k$ under different $R_L$.

results in substantially higher output power compared to operation at the natural resonant frequency.

Additionally, within the PT-symmetric region, decreasing load $R_L$ gradually increases the output power until a maximum value is reached. By comparing Fig. 3(b) with Fig. 3(a), it can be observed that whether the system operates within the exact or broken PT-symmetric regions, achieving the maximum output power inevitably decreasing the efficiency. And Fig. 3(c) clearly shows that the operating frequency is constant and changeable in the broken and exact PT regions, respectively. Besides, the coupling coefficient at the boundary between the two regions is denoted as $k_c$, which is not a constant but will vary with the $R_L$.

As illustrated in Fig. 4, the curves of output power and transfer efficiency for the WPT system across the full coupling coefficient range ($k = 0\sim1$) under varying loads are presented. The solid lines represent the operation at the natural resonant frequency, while the dashed lines indicate operation at the splitting frequency. According to (3), different loads correspond to distinct critical coupling coefficients $k_c$. It is evident that working at natural resonant frequency, the output power and transfer efficiency of the WPT system exhibit mutual constraints. Although the transfer efficiency remains high within the strong coupling interval, the output power is significantly low, leading to poor utilization of bus voltage. Even with a reduction in $R_L$, the bus voltage utilization remains poor. Conversely, when the system operates at the splitting frequency and as $k>k_c$, the output power markedly increases and becomes independent of the coupling coefficient, while maintaining high transfer efficiency. This advantageous characteristic offers a potential solution to the issue of weak output power capacity in strongly coupled WPT systems.

Within the exact PT-symmetry region, the preset resonant frequency will be split indicating that the frequency splitting phenomenon occurs. As load resistance $R_L$ decreases, the coupling coefficient $k_c$ also diminishes, indicating an expansion of the PT-symmetry region. For a given WPT system, the boundary of its PT-symmetry region will vary with the load resistance $R_L$. In addition, the critical coupling coefficient $k_c$ should be characterized not only by the coupling coefficient $k$, but also by the load conditions $R_L$.

### C. Input-to-Output Voltage Transfer Ratio $G_{vv(\omega)}$ Versus the Operating Frequency

The $G_{vv(\omega)}$ can be expressed in (12), where $Z_p$ and $Z_s$ are impedances of primary and secondary networks, respectively,

$$\begin{cases} G_{vv(\omega)} = \dfrac{\omega k\sqrt{L_pL_s}R_L}{Z_pZ_s+\omega^2k^2L_pL_s} \\ Z_p = j\omega L_p + \dfrac{1}{j\omega C_p} + R_p \\ Z_s = j\omega L_s + \dfrac{1}{j\omega C_s} + R_s + R_L \end{cases}. \tag{12}$$

As shown in Fig. 5(a), the frequencies of constant-voltage (CV) points $\omega_H = \frac{\omega_0}{\sqrt{1-k}}$ and $\omega_L = \frac{\omega_0}{\sqrt{1+k}}$ can be obtained by solving $\frac{\partial G_{vv(\omega)}}{\partial R_L} = 0$, which means the proposed system can work at the $R_L$-independent point [9].

Based on (3), two ZPA splitting frequencies $\omega_{PT\text{-}H}$ and $\omega_{PT\text{-}L}$ within the PT-symmetric region can be obtained as

$$\begin{cases} \omega_{PT-H} = \omega_0\sqrt{\dfrac{2-Q_s^{-2}+\sqrt{(2-Q_s^{-2})^2+4(k^2-1)}}{2(1-k^2)}} \\ \omega_{PT-L} = \omega_0\sqrt{\dfrac{2-Q_s^{-2}-\sqrt{(2-Q_s^{-2})^2+4(k^2-1)}}{2(1-k^2)}} \end{cases}. \tag{13}$$

Hence, the frequency splitting curve can be plotted in Fig. 5(b) when the $R_L$ is reduced from 150 to 20 Ω. The decrease of $R_L$ causes a leftward shift of the frequency splitting curve, approaching the CV points $\omega_H$ and $\omega_L$ in Fig. 5(b). Based on (4) and (5), the $G_{vv(\omega)}$ when the system is in the exact PT-symmetric region can be derived in (14), which is approximately equal to 1, corresponding to the frequency points $\omega_{PT\text{-}H}$ and $\omega_{PT\text{-}L}$ with the $k$-independent characteristic

$$\frac{\boldsymbol{V}_{\boldsymbol{PT-fs}}}{\boldsymbol{V}_{\boldsymbol{PT-fp}}} = \frac{\boldsymbol{I}_{\boldsymbol{PT-fs}}R_L}{\boldsymbol{I}_{\boldsymbol{PT-fp}}R_N} = \sqrt{\frac{L_p}{L_s}}\frac{R_L}{\frac{L_p}{L_s}(R_L+R_s)+R_p} \approx 1. \tag{14}$$

However, it is important to note that CV points $\omega_H$ and $\omega_L$ do not satisfy the ZPA condition. Hence, rather than operating at the CV points $\omega_H$ or $\omega_L$, slightly shifting the operating frequency to the $\omega_{PT\text{-}H}$ or $\omega_{PT\text{-}L}$ could meet the ZPA condition and the same voltage transfer ratio without compromising the transfer efficiency.

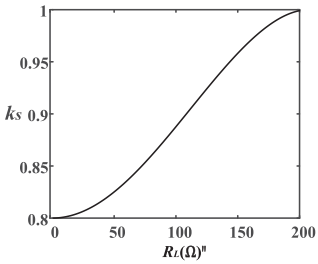


Fig. 6. Corresponding coupling coefficient $k_s$ versus $R_L$ on the condition $\omega_{PH\text{-}H} = 3\omega_{PH\text{-}L}$.

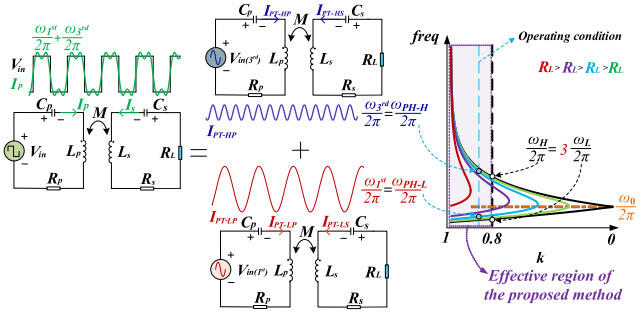


Fig. 7. Principle of aligning the first/third harmonic frequencies with the lower and upper splitting frequencies.

### D. Aligning the First/Third Harmonic Frequencies With the Lower and Upper Splitting Frequencies

As illustrated in (15), the full-bridge inverter generates the square wave voltage $V_{fin}$, which encompasses the first, third, and other odd harmonics by using the Fourier series expansion. And the energy contained in harmonics decreases as the harmonic order increases

$$\boldsymbol{V_{in}} = \boldsymbol{V_{fin}} + \frac{1}{3}\boldsymbol{V_{3fin}} + \frac{1}{5}\boldsymbol{V_{5fin}} + \ldots. \tag{15}$$

Within the exact PT-symmetric region and when $k<=0.8$, only one splitting frequency can be used to enhance the output power. When $k$>0.8, the first and third harmonics of $V_{fin}$ can be tuned to align the lower $\omega_{PT\text{-}L}$ and upper $\omega_{PT\text{-}H}$ splitting frequencies to further augment the output power capability as shown in Fig. 7. Thus, the $\omega_{PT\text{-}L}$ and $\omega_{PT\text{-}H}$ meet the relationship in (16). It should be noted that the two splitting frequencies possess the capability of transferring the same output power, indicating that the final output power of the system is the superposition of the power of first and third harmonics of the $V_{fin}$

$$\omega_{PT-H} = 3\omega_{PT-L}. \tag{16}$$

To satisfy the (16), the corresponding coupling coefficient $k_s$ for various load resistances $R_L$ can be calculated as

$$k_s = \sqrt{1 - \frac{9}{100}(2 - Q_s^{-2})^2}. \tag{17}$$

Given the condition $\omega_{PH\text{-}H} = 3\omega_{PH\text{-}L}$, in accordance with (17), the relationship between $R_L$ and $k_s$ is illustrated in Fig. 6. When either $R_L$ or $k$ of the system exceeds 0.8, system design can be conducted using the table lookup method, or it can serve as the control target for closed-loop control based on Fig. 6.

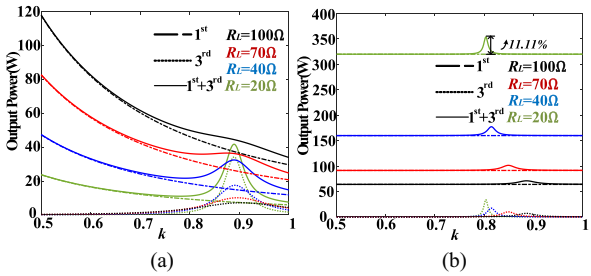


Fig. 8. Output power. (a) Working at the resonant frequency in the broken PT region. (b) Working at the splitting frequency in the exact PT region.

*Remark 1:* The effective region of the proposed method is $k$ = 0.8–1 for the following analysis. In Fig. 5(b), as $R_L$ decreases, the frequency splitting curves converge gradually. Compared to Fig. 5(a), at the same $k$, the ZPA splitting frequencies approaches CV points. This characteristic is shown in the operating frequency selection strategy in Fig. 7. Where the CV working point frequencies $\omega_H$ and $\omega_L$ (in black curve) satisfying the threefold relationship at the same $k$ is the critical interval, as derived from (18). When $R_L$ increases, $k$ needs to increase properly to meet the threefold relationship of $\omega_{PH\text{-}H}$ and $\omega_{PH\text{-}L}$.

Therefore, based on the proposed method, there are two design schemes.

1) For contactless slipring systems, due to spatial constrains, a very short transmission distance is typically required to eliminate contact friction. When the system operates stably with minimal variations in its operational state, $R_L$ can be considered approximately constant. According to the method presented in this letter, the value of $k$ can be selected within the range of 0.8 to 1.
2) For wireless In-wheel motor drive system, $k$ depends on the vehicle's design, and the equivalent impedance $R_L$ of motor changes with different operating conditions. When the coupling coefficient $k$ exceeds 0.8, dc–dc converter can be added on the secondary side to adjust the equivalent load $R_L$ and meet the design goals. This is a closed-loop system designed to control the equivalent resistance. After determining the parameter $k$, the target equivalent resistance value is referenced from Fig. 6. By adjusting the duty cycle of dc–dc converter, the system can automatically optimize and track the desired operating point

$$\omega_H = 3\omega_L \rightarrow \frac{\omega_0}{\sqrt{1-k}} = \frac{3\omega_0}{\sqrt{1+k}} \rightarrow k = 0.8. \tag{18}$$

In the broken PT region, by applying the voltage superposition theorem along with the voltage transfer ratio $G_{vv(\omega)}$ from (12), the output power $P_{N\text{-}L}$ working at the resonant frequency by combining the first and third harmonics can be derived by (19). Then the output power $P_{N\text{-}L}$ can be plotted in Fig. 8(a) with $R_L$ changing from 20 to 100 Ω

$$P_{N-L} = \frac{[G_{vv(\omega_0)}V_{in}]^2}{R_L} + \frac{\left[\frac{1}{3}G_{vv(3\omega_0)}V_{\text{in}}\right]^2}{R_L}. \tag{19}$$

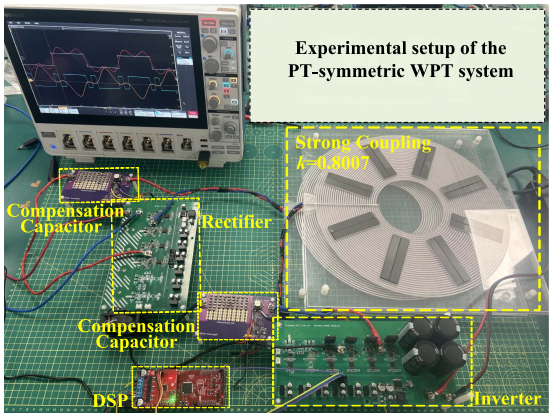


Fig. 9. Experimental setup of the PT-symmetric WPT system.

TABLE II
EXPERIMENT PARAMETERS

| Item | Value | Item | Value |
|---|---|---|---|
| $L_p/L_s$ | 305.6/304.9 uH | $V_{in}$ | 80 V |
| $R_p/R_s$ | 0.82/0.83 Ω | $k$ | 0.8–1 |
| $C_p/C_s$ | 12.75 nF | $R_L$ | 0–50 Ω |

In the exact PT region, the first harmonic is set to match the lower splitting frequency. Using the superposition theorem, output power $P_{PT\text{-}L}$ can be derived as (20). Comparison reveals that output power significantly increases under PT compared to natural resonance in Fig. 8(b). To further enhance output power, $k$ can be chosen according to (17) for a specific resistance $R_L$, causing the third harmonic frequency to align with the upper splitting frequency. Thus, output power $P_{PT\text{-}L}$ can be derived in (21), which $G_{vv(3\omega PT\text{-}L)} = G_{vv(\omega PT\text{-}H)}$ is equal to 1 based on (14). Both the first and third harmonics can be fully utilized to enhance the output power by 11.11% in Fig. 8(b)

$$P_{PT-L} = \frac{\left[G_{vv(\omega_{PT-L})}V_{\text{in}}\right]^2}{R_L} + \frac{\left[\frac{1}{3}G_{vv(3\omega_{PT-L})}V_{\text{in}}\right]^2}{R_L} = \frac{{V_{\text{in}}}^2}{R_L} + \frac{\left[\frac{1}{3}G_{vv(3\omega_{PT-L})}V_{\text{in}}\right]^2}{R_L} \tag{20}$$

$$P_{PT-L} = \frac{{V_{\text{in}}}^2}{R_L} + \frac{\left[\frac{1}{3}G_{vv(\omega_{PT-H})}V_{\text{in}}\right]^2}{R_L} = \frac{{V_{\text{in}}}^2}{R_L} + \frac{\frac{1}{9}{V_{\text{in}}}^2}{R_L} = \frac{10{V_{\text{in}}}^2}{9R_L}. \tag{21}$$

Additionally, in the exact PT region, the efficiency of splitting frequencies $\omega_{PH\text{-}L}/\omega_{PH\text{-}L}/\omega_{PH\text{-}H}+\omega_{PH\text{-}L}$(first/third/first + third) remains constant and equivalent based on (7).

## III. EXPERIMENTAL VERIFICATION

The experimental platform is built in Fig. 9, and the key parameters considering the influence of ferrites can be listed in Table II. $R_L$ and $k$ are set to 10 Ω and 0.8007 based on (17). In Fig. 10, the voltage ($\boldsymbol{V_p}$ and $\boldsymbol{V_s}$) and current ($\boldsymbol{I_p}$ and $\boldsymbol{I_s}$) waveforms of wireless link can be obtained under three typical cases, namely, setting the inverter working frequency

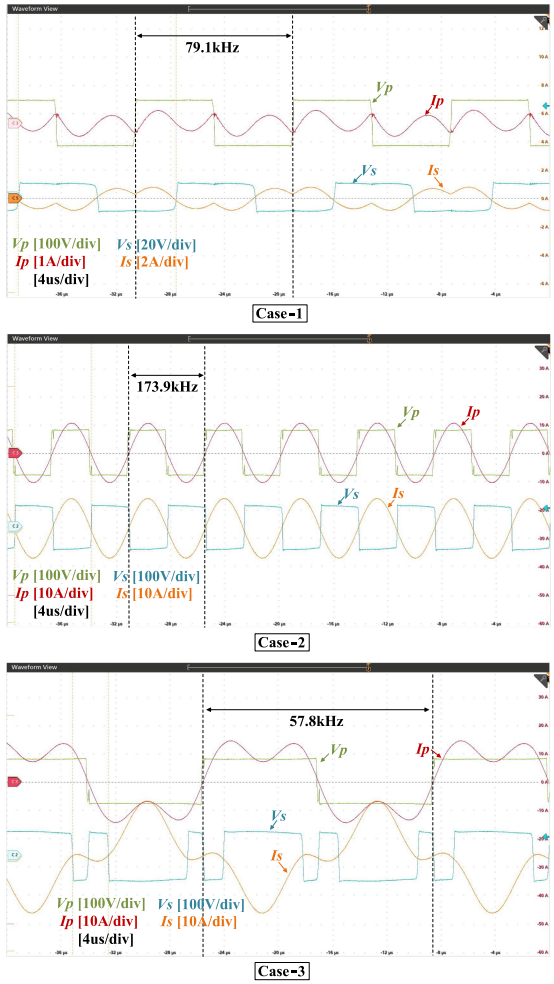


Fig. 10. Waveforms of the resonant voltages and currents when the system operates in different scenarios.

TABLE III
EXPERIMENT RESULTS

| | Frequency | Output power | Efficiency |
|---|---|---|---|
| Case-1 | 79.1 kHz | 4.9 W | 89.91% |
| Case-2 | 173.9 kHz | 560.7 W | 87.62% |
| Case-3(proposed) | 57.8 kHz | 609.2 W | 87.04% |

to the natural resonant frequency of 79.1 kHz (case 1), and to the upper/lower splitting frequency of 173.9 kHz (case 2)/ 57.8 kHz (case 3). The experiment results are presented in Table III. In case 1, the serious distortion of $\boldsymbol{I_p}$ and $\boldsymbol{I_s}$ is attributed to the substantial increase of $G_{vv}(3\omega_0)$. In case 2, by adopting upper splitting frequency, $\boldsymbol{V_p}$ and $\boldsymbol{I_p}$ are equal to $\boldsymbol{V_s}$ and $\boldsymbol{I_s}$, respectively, which is crucial for the applications of dc Transformer. In case 3, the current $\boldsymbol{I_p}$ becomes a saddle wave pattern indicating the full utilization of both the first and third harmonics.

*Remark 2:* The method proposed in this letter enables the realization of ZVS. As illustrated in Fig. 5, upon the strongly coupled WPT system entering the exact PT-symmetric region, the system exhibits three ZPA frequency points, corresponding to the natural resonant frequency and the lower and upper splitting

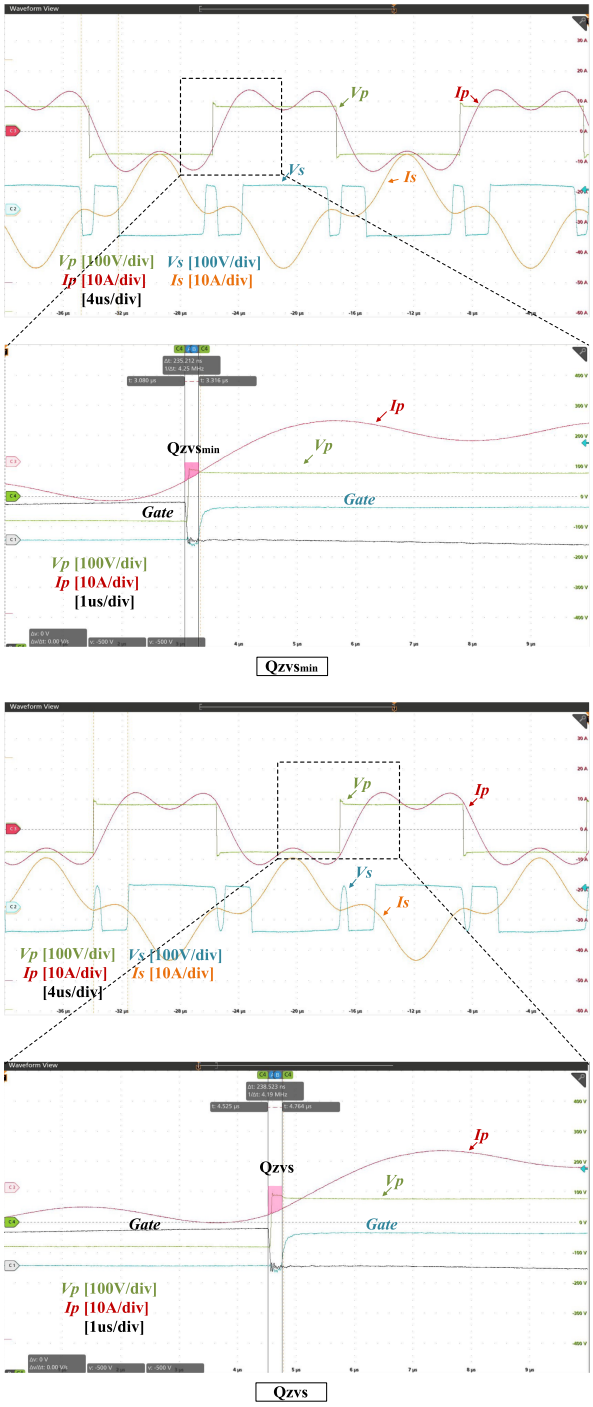


Fig. 11. Verification of ZVS operation.

frequencies, respectively. More significantly, after the superposition of the lower and upper splitting frequencies components, the circuit remains in the ZPA state as per the superposition theorem and case 3 illustrated in Fig. 10 of the experimental results. The condition for achieving ZVS in the MOSFET-based full-bridge converter is totally discharging the switch equivalent output capacitance $C_{\rm oss}$ during the deadtime $t_d$ before the corresponding switch turns on. To achieve ZVS, it is necessary to increase the frequency further based on ZPA operation to introduce an inductive reactive power component. Additionally, the critical condition for ZVS is influenced by the deadtime $t_d$. A deadtime that is too short will fail to achieve ZVS, while a deadtime that is too long can lead to conduction loss of body diode. Consequently, according to (22), it is essential to accurately calculate the deadtime $t_d$ at the critical condition of ZVS.

$$\left|\int_0^{t_d} i_p dt\right| \geq \int_0^{V_{\rm in}} C_{\rm oss} dv = Q_{\rm ZVSmin}. \tag{22}$$

The ZVS boundary condition ($Q$zvsmin) of the system with parameters $k = 0.8007$, $R_L = 10\,\Omega$, and $t_d = 238$ ns is calculated using (22). The experimental results are presented in Fig. 11. When $Q$zvs exceeds $Q$zvsmin, the conduction loss will increase due to the body diode of the switching transistor. Therefore, precise calculation of the deadtime is crucial for further enhancing system efficiency.

## IV. Conclusion

In this letter, a novel power-boosting strategy is proposed to solve the issue of low output power of the PT-symmetric WPT system. When $k$ exceeds 0.8, first/third harmonics frequencies of square voltage are aligned with the lower and upper splitting frequencies, respectively. Experimental results show that the proposed strategy achieves the output power of 609.2 W and transfer efficiency of 87.04%, which is a huge improvement compared to 4.9 W and 89.91% at the natural resonant frequency.

## References

[1] A. Abdolkhani and A. P. Hu, "Improved coupling design of contactless slipring for rotary applications," *IEEE J. Emerg. Sel. Topics Power Electron.*, vol. 3, no. 1, pp. 288–295, Mar. 2015.

[2] Y. Zhang, X. Li, S. Chen, and Y. Tang, "Soft switching for strongly coupled wireless power transfer system with 90° dual-side phase shift," *IEEE Trans. Ind. Electron.*, vol. 69, no. 1, pp. 282–292, Jan. 2022.

[3] Y. Zhang, Z. Yan, T. Kan, Y. Liu, and C. C. Mi, "Modelling and analysis of the distortion of strongly-coupled wireless power transfer systems with SS and LCC–LCC compensations," *IET Power Electron*, vol. 12, pp. 1321–1328, 2019.

[4] Y. Zhang, T. Kan, Z. Yan, Y. Mao, Z. Wu, and C. C. Mi, "Modeling and analysis of series-none compensation for wireless power transfer systems with a strong coupling," *IEEE Trans. Power Electron.*, vol. 34, no. 2, pp. 1209–1215, Feb. 2019.

[5] Y. Zhang, Z. Yan, Z. Liang, S. Li, and C. Mi, "An LCL-N compensated strongly-coupled wireless power transfer system for high-power applications," in *Proc. IEEE Appl. Power Electron. Conf. Expo*, 2019, pp. 3088–3091.

[6] L. Lai, B. Zhang, J. Lin, and Z. Wei, "On hamiltonian for PT-symmetric second-order circuits," *IEEE Trans. Circuits Syst. II, Exp. Briefs*, vol. 71, no. 5, pp. 2859–2863, May 2024.

[7] B. Zhang, W. Han, B. Cao, W. Hu, and Y. Hu, "Optimum design of wireless power Transfer-based snubbers for SiC MOSFET switching oscillations," *IEEE Trans. Power Electron.*, vol. 39, no. 9, pp. 10710–10715, Sep. 2024.

[8] J. Zhou, B. Zhang, W. Xiao, D. Qiu, and Y. Chen, "Nonlinear Parity-time-symmetric model for constant efficiency wireless power transfer: Application to a drone-in-flight wireless charging platform," *IEEE Trans. Ind. Electron.*, vol. 66, no. 5, pp. 4097–4107, May 2019.

[9] J. Liu, X. Qu, Y. Li, and C. Ma, "Investigation of PT-symmetric frequency and compensation for IPT coupling-independent CC/CV and efficiency in wide load range," *IEEE Trans. Power Electron.*, vol. 38, no. 11, pp. 13353–13362, Nov. 2023.